Tellus (1985), *37A*, 163–175

Mesoscale cellular convection: is it convection?

By BRIAN H. FIEDLER[1], *Advanced Study Program, National Center for Atmospheric Research*[2], *P.O. Box 3000, Boulder, Colorado, 80307, USA*

(Manuscript received March 20; in final form July 4, 1984)

ABSTRACT

The three convective instability models that aim to account for the broad aspect ratio of mesoscale cellular convection (MCC) are compared with a simple analytical version of the mesoscale entrainment instability (MEI) model proposed by Fiedler (1984). The inadequacies of the convective models are demonstrated. In the MEI model, the MCC is generated from above by a mesoscale instability in the entrainment fluxes. MEI is able to account for the broad aspect ratio of MCC. However the predicted growth rate for MEI is only of order 10^{-5} s^{-1}, which may be too small to account for the amplitude of MCC. Tactics are discussed for making aircraft observations that could reveal whether MCC is generated by MEI or by convection within the mixed layer.

1. Introduction

Photographs of Earth taken from space often reveal an extensive cellular or honeycomb cloud pattern in marine strato-cumulus cloud decks (Agee and Dowell, 1974). The individual cells are typically 20 to 100 kilometers across. Krueger and Fritz (1961) published the first report of this phenomenon and offered the explanation that the cloud patterns result from organized thermal convection. Since then the cloud patterns and the associated convection have come to be known as mesoscale cellular convection or MCC.

The best documented cases of MCC are those that occurred during the 1975 Air Mass Transformation Experiment (AMTEX). The observations presented by Agee and Lomax (1978) and Rothermel and Agee (1980) show that the AMTEX MCC was nonpenetrative: the convection was confined to a mixed layer under a stable inversion. Rothermel and Agee (1980) report an aircraft measurement of mesoscale upwelling of about 0.5 m s^{-1} beneath the cloudy region of an AMTEX MCC cell. The structure of MCC has an obvious similarity to the hexagonal cellular convection that is observed in laboratory studies of thermal convection (Palm, 1975; Spiegel, 1971). These observations certainly lead us to consider that the mesoscale cloud cover in the observed MCC was generated by advection of water vapor from below.

However, the notion that MCC is simply a natural analog to laboratory convection does not explain a fundamental feature of MCC—the broad width of the convection cells. The classic Rayleigh analysis of convective instability in a uniform fluid layer bounded by rigid and perfect thermal conductors predicts the fastest growing cells (or modes) to have a width to depth ratio, or aspect ratio, of less than 3:1 (Chandrasekhar, 1961, p. 18). The modes with large aspect ratios are strongly damped due to the shear and inertia of the horizontal motion field. From the continuity equation we know that the ratio of the horizontal velocity to the vertical velocity is nearly proportional to the aspect ratio. The horizontal motion field does not release potential energy and so always detracts from the instability. Steady-state convection in laboratory conditions similar to those for Rayleigh's theory is observed to be composed of cells with aspect ratios of about 3:1 (Busse, 1978); only a modest increase in aspect ratio from 2:1 to 4:1 is observed to occur in laminar convective rolls as the Rayleigh number is

[1] Current affiliation: Center for Meteorology and Physical Oceanography, Massachusetts Institute of Technology, Cambridge, MA, 02139, USA.

[2] The National Center for Atmospheric Research is sponsored by the National Science Foundation.

increased from the critical value to about ten times the critical value (Willis et al., 1972). This broadening phenomenon does not seem to be relevant to MCC. The convection cells of MCC are extremely flat, the aspect ratio of MCC is typically 30:1 (Agee and Dowell, 1974). Cumulus convection displays an aspect ratio of about 3:1 (Palm, 1975) and is a more appropriate phenomenon to compare with Rayleigh theory and laboratory results. The horizontal scale of MCC is distinct from the cumulus scale; the mesoscale cloud patterns of MCC appear to be composed of many cumulus scale clouds.

In Section 2 we review three previously published convective theories for the generation of MCC. The convective theories for MCC employ modifications of the Rayleigh theory that offset the large inefficiency of convection at large aspect ratio. None of the convective models has gained wide acceptance; one obvious drawback is that they seem to disallow any cumulus scale convection in conditions where MCC occurs. In contrast to the convective models, Fielder (1984) proposes that MCC results from a mesoscale instability in the entrainment fluxes. The usual long wavelength inefficiency that would occur in a convective instability is eliminated entirely rather than circumvented. In Section 3, a greatly simplified version of the MEI model of MCC is presented. The MEI model compares favorably with observations of MCC and observations of the environment in which MCC occurs. A suggested strategy to obtain useful observations of MCC by aircraft is discussed in Section 4.

The linear models for MCC can say nothing about the tendency for hexagonal organization. Before we begin serious attempts to study the hexagonal organization of MCC in nonlinear models, we must first be sure we know what causes MCC. No discussion of the possible reasons for the hexagonal structure of MCC will be presented here.

2. Mesoscale convective instabilities in mixed layers

In this section a linear model is developed that is suitable for analyzing the three proposed convective theories for MCC. We denote mesoscale fluctuations of a quantity by a prime (′) and horizontal averages by an overbar (̄). The convection is assumed to be completely confined within a mixed layer; penetrative effects are excluded. Turbulent transport will be modeled by an eddy diffusivity that is constant with height; the transport properties of the surface layer will be modeled only implicitly by the lower boundary conditions. The derivation of the model equations then follows that of Chandrasekhar (1961, p. 87) with the following exceptions. A split form of the eddy diffusivity is used (Ray, 1965): the vertical diffusivity for all quantities is K, the horizontal diffusivity is mK. The rotation vector $\mathbf{\Omega}$ of the system is not required to be vertical. Also, solely for the purpose of discussing the work of Rosmond (1973), an additional buoyancy production term $w'Q$ is added to the heat equation to approximate latent heat release processes. The production term in the heat equation is written

$$-w'\frac{\partial\bar{\theta}}{\partial z}+w'Q$$

where θ is the virtual potential temperature.

The momentum and heat equations are nondimensionalized with the height of the mixed layer H used as the length scale and the vertical thermal diffusion time H^2/K used as the time scale. We seek separable, two-dimensional solutions for vertical velocity, potential temperature and vertical vorticity

$$w'=\frac{K}{H}W(z)\,e^{iax}\,e^{\sigma t} \tag{2.1}$$

$$\theta'=\frac{K^2}{g\alpha H^3}\Theta(z)\,e^{iax}\,e^{\sigma t} \tag{2.2}$$

$$\zeta'=\frac{K}{H^2}Z(z)\,e^{iax}e^{\sigma t}. \tag{2.3}$$

α is the volumetric coefficient of thermal expansion and g is the acceleration due to gravity. For the sake of discussion we allow Q to have a slight wavenumber dependence so that

$$Q=Q_0+\frac{Q_2}{a^2}. \tag{2.4}$$

Q_2 represents buoyancy generation that is more effective at small wavenumbers (assuming Q_2 is positive). The model equations are similar to those of Chandrasekhar (1961, p. 89),

$$(D^2-ma^2)(D^2-a^2-\sigma)\,W=a^2\Theta+\tau DZ+ia\phi\tau Z \tag{2.5}$$

$$\sigma\Theta = RW + SW/a^2 + (D^2 - ma^2)\Theta \tag{2.6}$$

$$\sigma Z = (D^2 - ma^2)Z + \tau DW + ia\phi\tau W \tag{2.7}$$

D is the nondimensional vertical derivative, $D \equiv \partial/\partial z$. The other symbols in (2.5)–(2.7) are

$$\phi \equiv \frac{\Omega_x}{\Omega_z}, \tag{2.8}$$

the Rayleigh number

$$R \equiv \frac{g\alpha H^4}{K^2}\left(-\frac{\partial\bar{\theta}}{\partial z} + Q_0\right), \tag{2.9}$$

a latent heat forcing parameter

$$S \equiv \frac{g\alpha H^4}{K^2} Q_2, \tag{2.10}$$

and the Taylor number

$$\tau^2 \equiv \left(\frac{2\Omega_z K}{H^2}\right)^2. \tag{2.11}$$

In order to solve (2.5)–(2.7) we need upper and lower boundary conditions on Θ, W, DZ and DW. The critical wavenumber of the instability is sensitive to the boundary conditions on Θ, so of primary importance to us is formulating a realistic boundary condition for Θ. The relation between the fluctuating heat flux at the boundaries and the temperature fluctuation at the boundaries can be expressed as

$$D\Theta \equiv \gamma_0\Theta \tag{2.12}$$

at $z = 0$ and

$$D\Theta \equiv -\gamma_1\Theta \tag{2.13}$$

at $z = 1$. Note that the height $z = 0$ is taken to be just above the surface layer and not the ocean surface. If the boundaries are perfect thermal conductors then $\gamma_0 = \gamma_1 = \infty$ and the thermal boundary conditions become ones of constant temperature or $\Theta = 0$. If the boundaries are perfect thermal insulators then $\gamma_0 = \gamma_1 = 0$ and the thermal boundary conditions become ones of constant heat flux or $D\Theta = 0$.

The ocean surface temperature does not significantly respond to mesoscale mixed layer fluctuations and so can be assumed to be a constant. A bulk transfer model for the surface layer then gives

$$\gamma_0 = \frac{HC_T U_{10}}{K} \approx 0.03. \tag{2.14}$$

The above numerical value for γ_0 is for AMTEX conditions: $U_{10} \approx 10$ m s^{-1} (Sheu and Agee, 1977), $H \approx 2$ km (Agee and Lomax, 1978) and $K \approx w^*H \approx 1000$ m^2 s^{-1} (Sheu and Agee, 1977) where w^* is the convective velocity scale. Also, over the ocean surface the transfer coefficient $C_T \approx 1.5 \times 10^{-3}$ (Liu et al., 1979). The lower thermal boundary condition to mesoscale convection is closer to the perfectly insulating limit ($\gamma_0 = 0$) than to the perfectly conducting limit ($\gamma_0 = \infty$). The value of γ_1 is left as an unknown for now, but we assume $\gamma_1 \ll 1$.

2.1. *Perturbation solution of the model equations*

Since the magnitude of both γ_0 and γ_1 are much less than unity, the solution of (2.5)–(2.7) can be easily obtained by regular perturbation methods in which a^2 serves as the perturbation parameter. The analysis turns out to be restricted to nearly vertically uniform solutions for Θ. Busse and Riahi (1980) solved (2.5)–(2.7) for no rotation ($\tau^2 = 0$), marginal stability ($\sigma = 0$), and nearly insulating boundaries ($\gamma_0 = \gamma_1 \ll 1$) as a basis for further nonlinear solutions. Their linear work is easily expanded to allow for $\tau^2 \ll 1$, $|\sigma| \ll 1$ and γ_0 not equal to γ_1. Using essentially their method, (2.5)–(2.7) are solved in the Appendix with application of stress-free boundaries or $DZ = D^2W = 0$. The growth rate σ is determined to be

$$\sigma = \sigma_0 + m\left(\frac{R - R_c}{R_0}\right)a^2 - fa^4 \tag{2.15}$$

where

$$\sigma_0 \equiv -\gamma_0 - \gamma_1 + \frac{S}{120}, \tag{2.16}$$

$$R_0 \equiv 120m, \tag{2.17}$$

$$R_c \equiv R_0(1 + \tfrac{31}{89}\tau^2) \tag{2.18}$$

and

$$f \equiv m[\tfrac{34}{336}(m + 1) - \tfrac{31}{5544}m]. \tag{2.19}$$

In (2.15), σ_0 results from the influence of thermal boundary conditions and the wavenumber-dependent part of the latent heat release forcing term. In this analysis $W \approx a^2\Theta$ as $a \to 0$ due to viscous dissipation of the horizontal motion. Therefore the second term on the right hand side of (2.15) contains the effect of advection of sensible heat and the analogous latent heat advection as well as lateral heat diffusion. The a^4 term in (2.15) contains higher order corrections to the lower order estimate of Θ and the vertical velocity that it generates. The lowest order solution overestimates Θ because horizontal diffusion does not affect the lowest order. Fig. 1 is a plot of $\sigma - \sigma_0$ versus $\log(a)$ for $(R - R_c)/R_0$ equal to 1, 0, and -1; the anisotropy coefficient m has been set equal to unity. σ always becomes negative at large wavenumbers due to the a^4 term, which reflects lateral diffusion. σ can become positive at intermediate wavenumbers if $R > R_c$ due to the familiar convective instability. σ will be positive as $a \to 0$ only if σ_0 is positive. The physical meaning of positive σ_0 will be discussed later.

If both γ_1 and γ_0 are independent of wavenumber and $R > R_c$, then from (2.15) the mode with the largest growth rate has a wavenumber given by

$$a_m = \left[\frac{m}{2f}\left(\frac{R - R_c}{R_0}\right)\right]^{1/2}. \tag{2.20}$$

However, the growth rate σ of the corresponding mode would be positive only if R were sufficiently larger than R_c of if σ_0 were positive. It turns out that, for positive σ, a_m is always greater than the critical wavenumber a_c, which is the wavenumber of the unstable mode requiring the smallest Rayleigh number (Fig. 2). Physically the inertial inefficiency caused by the inertia of the horizontal motion (motion which does not generate buoyancy) is decreased at larger wavenumbers so a_m increases as R or σ increases. Therefore a_c is the smallest

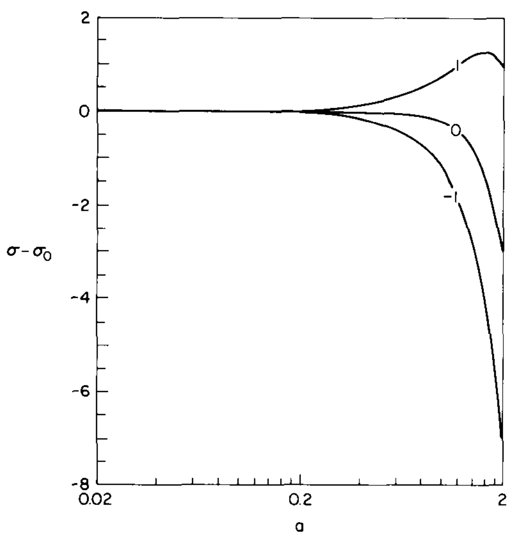

Fig. 1. Dimensionless growth rate of mesoscale mixed-layer convection. The growth rate σ of the convective instability minus the small wavenumber limit of the growth rate σ_0 as a function of wavenumber a. Curves are plotted for $(R - R_c)/R_0$ equal to 1, 0 and -1. For $(R - R_c)/R_0 < 0$ the largest growth rate occurs as $a \to 0$.

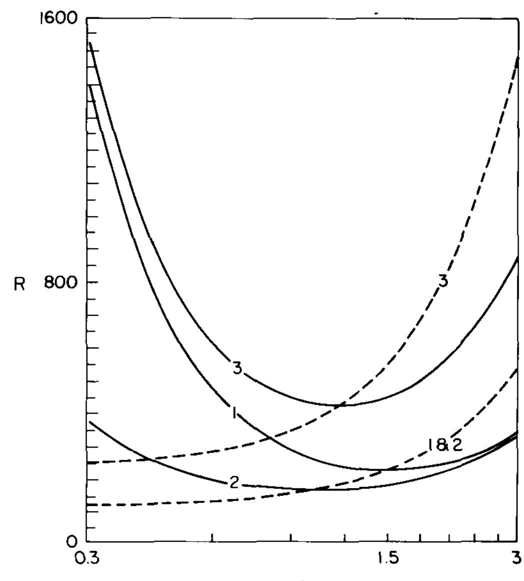

Fig. 2. Stability boundaries and most unstable modes for mesoscale mixed layer convection. The Rayleigh number R as a function of wavenumber (solid lines) for marginal stability ($\sigma = 0$). The wavenumber of the mode with largest growth rate (a_m) as a function of R (dotted lines). (1) poorly insulating boundaries ($\sigma_0 = -1$) and isotropic diffusion ($m = 1$); (2) better insulating boundaries or S taken to be positive ($\sigma_0 = -0.2$) and isotropic eddy diffusion ($m = 1$); (3) poorly insulating boundaries ($\sigma_0 = -1$) and enhanced lateral diffusion ($m = 2$). The growth rate σ is positive above the stability boundary (solid lines). The curve for the largest growth rate (dashed lines) intersects the stability boundary at the critical wavenumber a_c.

wavenumber that could ever be associated with the fastest positive growth rate. The critical wavenumber in (2.15) is given by

$$a_c = (-\sigma_0/f)^{1/4}. \quad (2.21)$$

If $\sigma_0 > 0$ and $R < R_c$ then both a_c and a_m would be zero.

From (2.20) and (2.21) and Fig. 1 and Fig. 2, it is apparent that the mode with the fastest positive growth can have a wavenumber much less than unity if R is slightly greater than R_c and σ_0/f is not too negative, or better yet, if R is less than R_c and σ_0 is positive.

2.2. *Broad convection due to insulating boundaries*

If m is taken to be unity and S is taken to be zero then (2.21) predicts the critical wavenumber for mesoscale convection to be

$$a_c = [5.1(\gamma_0 + \gamma_1)]^{1/4}. \quad (2.22)$$

Using the estimate for γ_0 in (2.14) and taking $\gamma_1 = 0$ as an extreme case of insulation, (2.22) predicts that a_c would be about 0.63, which corresponds to an aspect ratio of 10:1. γ_0 would have to be about 100 times smaller than the estimate in (2.14) in order for a_c to be 0.2 and correspond to the typical 30:1 aspect ratio of MCC. The estimate in (2.14) could not possibly be a factor of 100 too large.

The physical reason eq. (2.22) predicts a substantial decrease of a_c as $\gamma_0 + \gamma_1$ approaches zero is as follows: As the boundaries to the convection become insulating the lateral diffusion of heat becomes increasingly important in regulating the magnitude of Θ. In such circumstances the diffusive loss of buoyancy can be greatly diminished in modes of small wavenumber and the enhanced retention of buoyancy exactly offsets the dissipation due to shear at small wavenumbers. In the limit of perfectly insulating boundaries the Rayleigh number required for convective instability approaches a minimum constant R_c as $a \to 0$. This result was shown by Sparrow et al. (1964) and further elaborated on by Hurle et al. (1967). Sasaki (1971) made an attempt to apply these concepts to MCC. We will return to a discussion of the effect of thermal boundary conditions on mixed layer convection later in Section 2.5.

2.3. *Broad convection due to latent heat release*

If S is assumed to be positive, then σ_0 can be made positive and the small-wavenumber modes can be rendered the most unstable despite strongly dissipative thermal boundary conditions (i.e., $\gamma_0 + \gamma_1$ of order unity). Rosmond (1973) was able to predict convective modes of wavenumber as small as 0.1 to be the fastest growing in a linear convection model that included latent heat release. Apparently the success in predicting MCC-like scales to be the fastest growing was due to a subtle wavenumber dependency in the rather complicated latent heat release model. However the actual wavenumber dependency of the model seems to have been no more complicated than that offered in (2.4). Rosmond found it necessary to invoke a statically stable mean state that delicately balanced the latent heat release forcing so that the system was only marginally convectively unstable. The slight increase of efficiency of the latent heat release forcing at small wavenumbers could then have a critical effect on the balance and swing the balance in favor of instability at small wavenumbers. Using the terminology of the analysis presented here, Rosmond's MCC model seems to have employed large Q_0 and $\partial\bar{\theta}/\partial z \approx Q_0$ so that $R \approx R_c$. Q_2 was much less than Q_0, so the wavenumber dependence of Q was only slight. However, Q_2 was still large enough to make $\sigma_0 > 0$ because large values of Q_0 had been used. Therefore both a_m and a_c approached zero. Rosmond's model could offer a viable explanation for the aspect ratio of MCC if the increased efficiency of the latent heat forcing at small wavenumbers could be justified. However, neither adequate theoretical or experimental justification has been put forth. The appropriate value of Q_2 (and S) to use in modeling mixed layer convection is probably zero.

2.4. *Broad convection due to anisotropic eddy diffusion*

Another way to render small-wavenumber modes the most unstable in (2.15) is to assume the value of the m to be much greater than unity (Fig. 2). Priestley (1962) first proposed that if anisotropic eddy diffusion coefficients are included in a linear analysis of convective instability then the critical wavenumber a_c would be proportional to $m^{-1/2}$. Ray (1965) formally solved the stability problem proposed by Priestley, though the presentation of the results obscured any simple relation of the results to m. It was Williams (1972) who pointed out the validity of the Priestley hypothesis if m is much greater than 1. The critical wavenumber predicted in (2.21) is proportional to $m^{-1/2}$ as $m \to 0$ and so obeys the Priestley hypothesis. Physically, with enhanced lateral diffusion of heat and momentum the moderate wavenumber modes are damped so the small wavenumber modes become relatively more unstable. Anisotropic eddy diffusion has enjoyed some popularity in the literature as an explanation for the flat dimensions of MCC (Agee, 1976; Rosmond, 1973; Atkinson, 1981). However, there has been little justification for assuming the required inordinate amount of anisotropy in the eddy diffusion coefficients, particularly in a convectively unstable mixed layer. If eddy anisotropy alone were to explain the disparity between the scale of MCC and the preferred scale in the Rayleigh problem ($a_c \approx 2$–3) then m would have to be about 100. However, if a convectively unstable mixed layer the vertical diffusion is enhanced by narrow plumes and thermals so the appropriate value for m might in fact be less than unity.

2.5. *Broad convection by boundary generation of buoyancy fluctuations*

Section 2.2 shows that insulating boundaries are not a likely cause of the large aspect ratio of MCC. Although a surface layer over an ocean can lead to $\gamma_0 \ll 1$, γ_0 is still not small enough. Even with $\gamma_1 = 0$ the predicted critical wavenumber is considerably greater than the wavenumber of MCC. We are led to consider the possibility that γ_1 is negative for MCC, therefore allowing $\sigma_0 > 0$ and $a_c = 0$. A negative value for γ_1 would imply that the heat fluxes at the upper boundary are generating the mesoscale buoyancy fluctuations rather than dissipating or insulating them. The vertical velocity field would not be needed to generate temperature fluctuations. If $\gamma_0 + \gamma_1$ is negative then the generation of mesoscale buoyancy fluctuations can be virtually uncoupled from the generation of momentum if the Rayleigh number is small. In that limit the growth rate of the temperature fluctuations is determined by the boundary conditions and the most unstable modes naturally occur at small wavenumbers because lateral diffusion is decreased at small wavenumbers. In Section 3 it is shown that γ_1 can be negative when the mixed layer is capped by cloud due to the effect cloud cover has on entrainment.

3. Mesoscale entrainment instability

Fiedler (1984) showed that the Lilly-type models for strato-cumulus capped mixed layers allow for a mesoscale instability in which mesoscale fluctuations of buoyancy and humidity are amplified in phase by entrainment. The instability is called mesoscale entrainment instability (MEI). Although the modes have the appearance of having been convectively generated, any mesoscale advection of heat or moisture within the mixed layer is a secondary process and does not contribute to the instability.

MEI occurs by the following process (Fig. 3): In general, thicker cloud cover at the top of a mixed layer tends to increase the rate of entrainment. Therefore entrainment is usually a process which tends to dissipate or stabilize fluctuations in cloud cover when the air above the mixed layer is drier than the mixed layer. However, if the temperature gradient in the stable layer is sufficiently great this tendency can be reversed. Regions with relatively more buoyant mixed-layer air will rise farther into

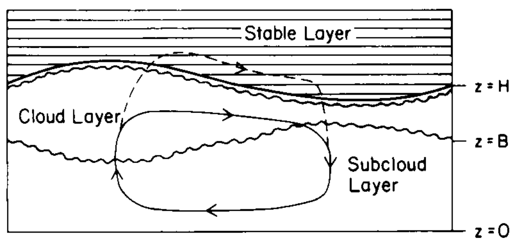

Fig. 3. Mesoscale entrainment instability. A positive buoyancy fluctuation rises into the stable layer and becomes adjacent to warmer air. A decreased mass entrainment flux occurs over the buoyancy fluctuation, resulting in the generation of a positive fluctuation in cloud thickness. The positive cloud thickness fluctuations in turn couple to the generation of the positive buoyancy fluctuations by latent heat release and by promoting the entrainment of buoyancy. Note that although less mass is entrained where the cloud is thicker, the air entrained is relatively warmer than that where the cloud is thinner. Therefore entrainment can reinforce mesoscale buoyancy fluctuations as well as mesoscale humidity fluctuations. The level temperature stratification in the stable layer is shown. The rotational flow of convection confined to the mixed layer is indicated by the solid line. The additional component of the flow pumped by the mesoscale fluctuation in the mass entrainment rate when MEI is occuring is indicated by the dashed line.

the overlying stable air as compared with the less buoyant mixed-layer air and the density decrease across the inversion can intensify above the more buoyant regions. As a result the mass entrainment rate can be decreased above positive mesoscale buoyancy fluctuations and fluctuations in the mixing ratio can thereby be generated in phase with the mesoscale buoyancy fluctuations. Mesoscale buoyancy fluctuations are generated by two mechanisms. First, the latent heat release associated with increased cloud thickness provides buoyancy. Secondly, although the mass entrainment rate decreases above the more buoyant regions, the production of buoyancy by entrainment can increase in those regions because the air entrained there is warmer than the air entrained into the less buoyant regions.

In this section we present a simplified, analytical version of the MEI model presented by Fiedler (1984). Although the growth rate of MEI was shown to increase as the mean cloud thickness increases, the mechanism of MEI can be most easily presented in the limit of infinitesimally thin cloud cover. We take that limit here so that no account needs to be made of latent heat release on the mesoscale buoyancy fluctuations. Also, the dynamics of the stable layer that cause the small-wavenumber cut-off will have to be excluded from the analysis.

As discussed in Section 2 in regards to convective instabilities, the boundary conditions in this problem are essentially ones of $|\gamma_0| \ll 1$ and $|\gamma_1| \ll 1$. Therefore we assume θ' and the total water mixing ratio fluctuations r' are perfectly well-mixed vertically throughout the mixed layer (except in the surface layer and θ' in the thin cloud layer). As in Fiedler (1984), all mesoscale advective transport of θ' and r' is ignored; the modeling effort is concentrated on the generation of MCC by the entrainment fluxes rather than by convection. Unlike the last section, the analysis in this section is conducted with dimensional quantities. Normal modes proportional to $e^{\sigma t} e^{ikx}$ are assumed. The conservation equation for a scalar s' (either θ' or r') is

$$\bar{H}\sigma s' = -H' \frac{\partial \bar{s}}{\partial t} - \bar{H}Kk^2 s' - C_T U_{10} s' + (w_e \Delta s)' \tag{3.1}$$

as in [2.6] and [2.7] of Fiedler (1984). The lower boundary fluxes are modeled by bulk transfer. The upper boundary fluxes are modeled as the entrainment velocity w_e times the jump in the quantity across the entrainment interface. Note $\Delta\theta$ must refer to the difference in θ above the entrainment interface and θ below the thin cloud layer. The fact that the downwards flux of buoyancy into the subcloud layer is still proportional to $w_e \Delta\theta$ despite the intervening cloud layer follows if the moist static energy and mixing ratio are conserved and well-mixed throughout the mixed layer.

The entrainment velocity w_e will be constrained using the entrainment closure assumption introduced by Kraus and Schaller (1978),

$$\int_{\text{neg}} F\, \mathrm{d}z = -E^2 \int_{\text{pos}} F\, \mathrm{d}z \tag{3.2}$$

where F is the vertical flux of virtual potential temperature. E is thought to be about 0.2 (Stull, 1976; Deardorff, 1976). When (3.2) is applied to the convective boundary layers of AMTEX, the negative buoyancy flux occurs only in a layer below the cloud base (Fiedler, 1984). The presence of a cloud layer of thickness χ will increase the entrainment velocity w_e by an amount that will cause the layer of negative buoyancy flux to expand downward by a distance comparable to χ and so leave the left-hand side of (3.2) nearly unchanged. Using (3.2) to lowest order in E and in cloud thickness χ

$$w_e = \frac{F_0}{\Delta\theta}\left(E + \frac{\chi}{H}\right) \tag{3.3}$$

where F_0 is the surface buoyancy flux. The bulk transfer model for F_0 is

$$F_0 = C_T U_{10} \delta\theta \tag{3.4}$$

where $\delta\theta$ is the drop in θ going up through the surface layer. In the limit of infinitesimally thin mean cloud cover $\bar{\chi}$

$$\bar{w}_e = E \frac{\bar{F}_0}{\Delta\bar{\theta}} \tag{3.5}$$

and

$$w_e' = \frac{-\bar{w}_e \Delta\theta'}{\Delta\bar{\theta}} - \frac{EC_T U_{10} \theta'}{\Delta\bar{\theta}} + \frac{\bar{F}_0 \chi'}{\Delta\bar{\theta}\bar{H}}. \tag{3.6}$$

Now χ' is the difference between the cloud height fluctuation and cloud base fluctuation

$$\chi' = H' - B'. \tag{3.7}$$

H' is generated in response to buoyant lifting from below. For sufficiently large k and small σ

$$H' = \frac{\bar{H}}{2\,\Delta\bar{\theta}}\,\theta' \tag{3.8}$$

(Fiedler, 1984). B' results from evaporation caused by θ' and condensation associated with r' (Fiedler, 1984). In these modes we find the second process is the most important,

$$B' = \frac{-r'}{\mu\Gamma} \tag{3.9}$$

where μ is the derivative of the saturation mixing ratio with respect to temperature

$$\mu \equiv \frac{\partial q_{\text{sat}}}{\partial T} \tag{3.10}$$

at cloud base temperature. Γ is the dry adiabatic lapse rate, $\Gamma = 10^{-2}$ K m^{-1}.

If k is not too small then the stable layer isotherms will remain nearly level despite any deflection of the entrainment interface (Fiedler, 1984). A positive fluctuation H' will bring the mixed layer adjacent to warmer air in the stable layer so

$$\Delta\theta' = \left.\frac{\partial\bar{\theta}}{\partial z}\right|_{H+} H' - \theta'. \tag{3.11}$$

A nondimensional virtual potential temperature gradient is defined

$$G \equiv \left.\frac{\partial\bar{\theta}}{\partial z}\right|_{H+} \frac{\bar{H}}{2\,\Delta\bar{\theta}}. \tag{3.12}$$

We assume that the gradient of mixing ratio in the stable layer is negligible so

$$\Delta r' = -r'. \tag{3.13}$$

We can now write w_e' in terms of θ' and r'

$$w_e' = \frac{-\bar{w}_e}{\Delta\bar{\theta}}(G-1)\,\theta' - \frac{EC_T U_{10}\theta'}{\Delta\bar{\theta}} + \frac{\bar{F}_0}{\Delta\bar{\theta}}\left(\frac{\theta'}{2\,\Delta\bar{\theta}} + \frac{r'}{\bar{H}\mu\Gamma}\right). \tag{3.14}$$

The stability model will be applied to an AMTEX mixed layer characterized by the following parameters:

$C_T = 1.5 \times 10^{-3}$ (Liu et al., 1979),

$U_{10} = 10$ m s^{-1} (Sheu and Agee, 1977)

$\delta\theta = 8$ K (Sheu and Agee, 1977)

$F_0 = 0.12$ K m s^{-1}

$H = 2 \times 10^{-3}$ m (Agee and Lomax, 1978)

$\left.\frac{\partial\bar{\theta}}{\partial z}\right|_{H+} = 2.0 \times 10^{-2}$ K m^{-1} (Agee and Lomax, 1978)

$\Delta\bar{\theta} = 2$ K (Jensen and Lenschow, 1978)

$w_e = 0.012$ m s^{-1}

$G = 10$

$\Delta\bar{r} = -4 \times 10^{-3}$ (Jensen and Lenschow, 1978)

$\mu = 3 \times 10^{-4}$ K^{-1}

The actual value of $\Delta\bar{\theta}$ is difficult to measure. The assumed value is slightly less than the value apparent in the sounding presented in Jensen and Lenschow where $\Delta\theta \approx 4$ K. Without such a low value for $\Delta\theta$ the growth rate of MEI would be negative (Fiedler, 1984). Anticipating the results that $r'/\theta' \approx 3.2 \times 10^{-3}$ K^{-1} we retain only the most important term in (3.14)

$$w_e' = \frac{-\bar{w}_e}{\Delta\bar{\theta}}\,G\theta'. \tag{3.15}$$

In solving for $(w_e\Delta\theta)'$ we must return to (3.6)

$$(w_e\Delta\theta)' = -EC_T U_{10}\theta' + \bar{F}_0\left(\frac{\theta'}{2\Delta\bar{\theta}} + \frac{r'}{\bar{H}\mu\Gamma}\right). \tag{3.16}$$

The mean buoyancy increases due to the convergence of the surface buoyancy flux and the entrainment buoyancy flux

$$\frac{\partial\bar{\theta}}{\partial t} = \frac{(1+E)}{\bar{H}}F_0. \tag{3.17}$$

From (3.5), (3.16) and (3.17)

$$(w_e\Delta\theta)' - H'\frac{\partial\bar{\theta}}{\partial t} = -EC_T U_{10}\theta' - \frac{\bar{w}_e\theta'}{2} + \frac{F_0 r'}{\bar{H}\mu\Gamma}. \tag{3.18}$$

From (3.1) we can now construct an eigenvalue problem with σ the eigenvalue and (r', θ') the eigenvector

$$(\sigma \bar{H} + C_T U_{10} + \bar{w}_e + \bar{H}Kk^2) r' + \frac{\bar{w}_e}{\Delta\bar{\theta}} G \Delta \bar{r} \theta' = 0 \quad (3.19)$$

$$\frac{F_0}{\bar{H}\mu\Gamma} r' - \left[\sigma \bar{H} + (1 + E) C_T U_{10} + \frac{\bar{w}_e}{2} + \bar{H}Kk^2\right] \theta' = 0. \quad (3.20)$$

In (3.19), the $H' \partial\bar{r}/\partial t$ term would be of order $H' \mu \partial\bar{\theta}/\partial t$ and so is negligible. The nontrivial solution of (3.19) and (3.20) occurs with an eigenvalue that makes the determinant of the eigenvector coefficients vanish. One additional approximation will make it particularly easy to write a solution for σ

$$(1 + E) C_T U_{10} + \tfrac{1}{2}\bar{w}_e = C_T U_{10} + \bar{w}_e. \quad (3.21)$$

From (3.19) and (3.20) we now have

$$\sigma \bar{H} + \bar{H}Kk^2 + C_T U_{10} + \bar{w}_e = \frac{F_0}{\Delta\bar{\theta}} \left(\frac{-EG\Delta\bar{r}}{\bar{H}\mu\Gamma}\right)^{1/2} = 6.3 \times 10^{-2}\,\mathrm{m\,s^{-1}} \quad (3.22)$$

in AMTEX conditions. Had we not assumed (3.21), there would be two real eigenvalues with magnitudes close to that in (3.22). For $k > 1.8 \times 10^{-4}\,\mathrm{m}^{-1}$, σ is negative. For a 30:1 aspect ratio mode, or $k = 1 \times 10^{-4}\,\mathrm{m}^{-1}$, the boundary driving is just barely able to overcome the lateral diffusion and the diffusion into the boundaries: $\sigma = 9.1 \times 10^{-6}\,\mathrm{s}^{-1}$ and $r'/\theta' = 3.2 \times 10^{-3}\,\mathrm{K}^{-1}$.

The growth rate predicted by (3.22) is slightly higher than that found in Fiedler (1984) for the same specified conditions. In that more complete model we would not find growth rates as large as $1 \times 10^{-5}\,\mathrm{s}^{-1}$ unless $\bar{\chi} = 500$ m or $\Delta\bar{\theta} = 1.2$ K. One reason for the difference is that at $k = 1 \times 10^{-4}\,\mathrm{m}^{-4}$ the dynamics causing the small-wavenumber cut-off are already significant. In the model of Fiedler (1984) the growth rate of MEI peaked at aspect ratios of about 30:1. In that model the isotherms in the stable layer do not remain level as k becomes small so (3.8) and (3.11) are overestimates for small k. The linear response of the velocity and temperature fluctuations in the stable layer are modes proportional to $e^{-\gamma z}$. Retaining the most important terms in equation [2.49] of Fiedler (1984) we have

$$\gamma^2 \approx \frac{N}{\bar{w}_e} k \quad (3.23)$$

where N is the Brunt frequency of the stable layer. From [2.52] of Fiedler (1984) we find that the small-wavenumber cut-off dynamics will dominate the solutions if

$$\gamma < \frac{1}{\Delta\bar{\theta}} \left.\frac{\partial\bar{\theta}}{\partial z}\right|_{H+}. \quad (3.24)$$

So in AMTEX conditions the small-wavenumber cut-off will severely damp the solutions if $k < 5 \times 10^{-5}\,\mathrm{m}^{-1}$ or if the aspect ratio is greater than 60:1. With diffusion causing a large-wavenumber cut-off, peak growth rates were found to occur at aspect ratios of about 30:1.

4. Summary

The previously proposed linear convective models for MCC are unrealistic. One requires more eddy anisotropy than the atmosphere could ever provide. Another requires more boundary insulation than could ever occur across a surface layer in the atmosphere. A third theory has been presented that is similar to the model of Rosmond (1973). The third theory includes subtle wave-number-dependent forcing that requires rather special conditions for it to dominate the dynamics. Even then, such a wavenumber-dependent forcing may not be justified.

Advocates of Rosmond's parameterized model could test it with a simple two-dimensional numerical simulation of moist, nonprecipitating convection. We note that van Delden and Oerlemans (1982) observed 15:1 aspect ratio clustering of cumulus elements in a two-dimensional numerical model of moist convection. However, they used extreme anisotropy in the diffusion of water vapor, i.e., the vertical diffusion of water vapor was zero., Since water vapor contributes to buoyancy via latent heat release, such an assumption for diffusion probably caused the convection to broaden for reasons discussed in Section 2.4.

In this paper I have shown that MCC does not have to be generated by a classical convective instability. A mesoscale entrainment instability is another possible source for MCC. MEI requires rather special circumstances to achieve substantial growth rates, namely a lack of radiative damping and small $\Delta\bar{\theta}$ despite the large $\partial\bar{\theta}/\partial z$ in the stable layer (Fiedler, 1984). The growth rate of MEI in (3.22) goes as the square root of the coefficient of χ/H in (3.3), so we may wish to consider an entrainment closure relation more sensitive to cloud cover than (3.2). However, more elaborate modeling of MEI or entrainment does not seem to be called for. MEI has been shown to be a theoretical possibility. Actual observations are required to convincingly demonstrate that MEI, rather than convection, is generating MCC.

The observation that MCC occurs only over water is clearly supported by (3.22). All else being the same, using a value of C_T of order 10^{-2} typical for a land surface (Garratt and Hicks, 1973) in (3.22) would cause σ to be negative due to diffusion of the buoyancy fluctuations into the lower boundary.

Sheu and Agee (1977) show that MCC was observed during AMTEX only when the surface windspeed and air-sea temperature difference was sufficiently large. This finding seems to indicate that the occurrence of MCC requires a threshold surface buoyancy flux F_0. The MEI model for MCC supports this observation both directly and indirectly. The direct reason is as follows. In (3.22) the growth rate has a positive contribution proportional to the surface buoyancy flux. The negative contribution due to horizontal diffusion is proportional to K, which in a convective boundary layer is proportional to the cube root of F_0. So not only is large F_0 required to bring into being an observable amplitude of MEI, but also a sufficiently large F_0 is required to make the growth rate positive. Indirectly, large values of F_0 simply indicate a significant or recent cold-air outbreak. Perhaps small values of $\Delta\bar{\theta}$ and large values of $\partial\bar{\theta}/\partial z$ in the stable layer are found only within about 1000 km of the cold front.

MCC occurs in the tropical trade-wind boundary layer as well as in cold-air outbreaks. In the tropics, F_0 and the stable layer temperature gradient are an order of magnitude smaller than those in the AMTEX environment. Clearly the modes of MEI discussed here would be stable in the tropics. However, in light of recent research by Randall (1984), it seems that another class of MEI modes are possible in the tropics. Randall (1984) has shown that entrainment can cause cloud thickness to increase when the large-scale subsidence is weak and the temperature and humidity difference is small across the entrainment interface. Randall presents data which shows these conditions existing in the south west region of the trade-wind boundary layer off California, precisely where MCC often occurs. Recall that in the AMTEX MEI modes discussed in this paper there was decreased mass entrainment above cloudy regions as a result of the large temperature gradient in the stable layer. In the conditions Randall describes, MEI would be possible with increased mass entrainment above cloudy regions. MEI could occur without the presence of a large temperature gradient in the stable layer. The quantitative details of the tropical MEI modes will be the subject of future work.

Further observations are needed to help reveal the source of MCC. Like ordinary convection, MEI also has a rotational convective circulation associated with it. Unlike ordinary convection, MEI has a strong horizontal flow above the entrainment interface that is pumped by the mesoscale variation in the entrainment rate (Fig. 3). Although an upwards velocity fluctuation is depicted going from the mixed layer to the stable layer above the cloudy region, the mean subsidence velocity plus the fluctuating velocity is always down through the entrainment interface—mixed layer air never becomes stable layer air. Otherwise the MEI circulation is somewhat similar to the penetrative circulation envisaged by Rothermel and Agee (1980). Mesoscale fluctuations in the entrainment velocity of order 1 cm s^{-1} would cause a horizontal streaming velocity of order 1 m s^{-1} in the lower 100 meters of the stable layer. Such magnitude velocities are easily detected by aircraft and should stand out above any background noise. Simple detection of the lateral streaming velocities in the stable layer will add credence to the MEI model.

To demonstrate conclusively that MEI is the primary cause of MCC would require knowledge of the relative strengths of the mesoscale entrainment fluxes and the convective fluxes effecting MCC. Making direct measurements of the entrainment fluxes and weak vertical velocities is difficult. Detecting mesoscale fluctuations in these quantities would be even more difficult.

An indirect strategy to obtain these fluxes would probably be best. Measurements from two simultaneous flights, one at 100 meters and one directly above at height $\bar{H}$, might be sufficient. By measuring the mesoscale fluctuations in the horizontal velocity the much weaker vertical velocities in the MCC circulation could be inferred. The upper level flight could penetrate the entrainment interface between the mesoscale crests and troughs and presumably could measure the streaming velocity and the depth of the shallow layer containing the streaming. Scale analysis of the continuity equation could then give w' at H. Evidence of steady state (small $\partial H'/\partial t$) would imply $w_e' = -w'$ at H. The jumps $\Delta\theta$ and Δr could also be obtained from the penetrations through the entrainment interface. The MEI model is very sensitive to the fluctuations of the temperature field in the stable layer and in particular to $\Delta\theta'$. Measurements of the temperature along the flight path while in the stable layer and knowledge of the vertical temperature gradient will give the shape of the isotherm contours in the stable layer and will allow $\Delta\theta'$ to be calculated. Subsequently the mesoscale entrainment fluxes $(w_e \Delta\theta)'$ and $(w_e \Delta r)'$ could be calculated.

The convective fluxes within the mixed layer could be calculated if the mesoscale fluctuations in water vapor and buoyancy were known. Since these quantities are vertically well-mixed, the convective velocities and mesoscale scalar fluctuations could be obtained by the parallel low level flight. The mesoscale convective and entrainment fluxes could then be compared. Hopefully the source of the mesoscale buoyancy and moisture fluctuations in MCC would then at last be revealed.

5. Acknowledgements

This work is largely the result of my doctoral dissertation research conducted at the University of Colorado. I thank my thesis advisor Prof. Juri Toomre for nurturing my interest in thermal convection. I thank Prof. Toomre, Dr. Donald Lenschow, Dr. Margaret Le Mone, Dr. Christopher Bretherton and Dr. David Randall for commenting on earlier versions of this work. I thank two anonymous reviewers for their professional reviews. I thank Dr. Donald Lenschow for advice on observational strategies.

The work was supported in part at the University of Colorado by the National Aeronautics and Space Administration through contract NAS8-31958 and grant NSG-7511.

6. Appendix. Perturbation solution for small-wavenumber convective instability in a fluid layer

To solve (2.5)–(2.7) we will use a perturbation parameter ε and write all the variables in (2.5)–(2.7) as a product of an O(1) variable (Nayfeh, 1973, p. 8) and ε to a power

$$a^2 \equiv \varepsilon^2 \eta^2, \tag{A.1}$$

$$W \equiv \varepsilon^2 \eta^2 V, \tag{A.2}$$

$$\tau \equiv \varepsilon T, \tag{A.3}$$

$$S \equiv \varepsilon^4 C, \tag{A.4}$$

$$Z \equiv \varepsilon^2 \eta^2 X, \tag{A.5}$$

$$\sigma \equiv \varepsilon^4 s, \tag{A.6}$$

$$\gamma_0 \equiv \varepsilon^4 b_0, \tag{A.7}$$

$$\gamma_1 \equiv \varepsilon^4 b_1. \tag{A.8}$$

Further, we redefine the nondimensional vertical coordinate as

$$y \equiv 2(z - \tfrac{1}{2}) \tag{A.9}$$

so the upper boundary is at $y = 1$ and the lower boundary is at $y = -1$.

Making the above substitutions, (2.5)–(2.7) become

$$(4D_y^2 - m\varepsilon^2 \eta^2)\,\Theta = \varepsilon^4 s\Theta - \varepsilon^2 \eta^2 RV - \varepsilon^4 CV, \tag{A.10}$$

$$\begin{aligned}(4D_y^2 - \varepsilon^2 \eta^2)(4D_y^2 - m\varepsilon^2 \eta^2)\,V &= s\varepsilon^4(4D_y^2 - m\varepsilon^2 \eta^2)\,V + \Theta + \varepsilon^2 TDX \\ &\quad + \varepsilon^3 i\eta\phi TX,\end{aligned} \tag{A.11}$$

and

$$(4D_y^2 - m\varepsilon^2 \eta^2)\,X = \varepsilon^4 sX - TDV - \varepsilon i\eta\phi TV \tag{A.12}$$

where

$$D_y \equiv \frac{\partial}{\partial y} = \tfrac{1}{2} D. \tag{A.13}$$

The boundaries are taken to be rigid and stress-free, so

$$V = 0 \quad \text{at } y = -1 \text{ and } y = 1, \tag{A.14}$$

$$D_y^2 V = 0 \quad \text{at } y = -1 \text{ and } y = 1, \tag{A.15}$$

and

$$D_y X = 0 \quad \text{at } y = -1 \text{ and } y = 1. \tag{A.16}$$

The thermal boundary conditions (2.12) and (2.13) become

$$2D_y\Theta = \varepsilon^4 b_0 \quad \text{at } y = -1 \tag{A.17}$$

and

$$2D_y\Theta = -\varepsilon^4 b_1 \quad \text{at } y = 1. \tag{A.18}$$

The solution of (A.10)–(A.12) is sought in the form

$$R = \sum \varepsilon^n R_n, \tag{A.19}$$

$$\Theta = A \sum \varepsilon^n \Theta_n, \tag{A.20}$$

$$V = A \sum \varepsilon^n V_n, \tag{A.21}$$

$$X = A \sum \varepsilon^n X_n. \tag{A.22}$$

The order ε^0 equations from (A.10)–(A.12) are

$$D_y^2\theta_0 = 0, \tag{A.23}$$

$$16D_y^4 V_0 = \Theta_0, \tag{A.24}$$

$$2D_y^2 X_0 = -TD_y V_0, \tag{A.25}$$

which yield solutions satisfying (A.14)–(A.18)

$$\Theta_0 = 1, \tag{A.26}$$

$$V_0 = \frac{1}{16 \times 4!}(y^4 - 6y^2 + 5), \tag{A.27}$$

$$X_0 = \frac{-T}{32 \times 5!}(y^5 - 10y^3 + 25y). \tag{A.28}$$

The relevant order ε^2 equations are

$$4D_y^2\Theta_2 = m\eta^2\Theta_0 - \eta^2 R_0 V_0 \tag{A.29}$$

and

$$16D_y^4 V_2 = (4m+1)\eta^2 D_y^2 V_0 + \Theta_2 + 2TD_y X_0. \tag{A.30}$$

We define the vertical averaging operator $\langle\ \rangle$ as

$$\langle\ \rangle \equiv \tfrac{1}{2}\textstyle\int \mathrm{d}y. \tag{A.31}$$

$D_y\Theta_2 = 0$ at the boundaries, so upon operating on (A.29) by $\langle\ \rangle$,

$$R_0 = \frac{\langle\Theta_0\rangle}{\langle V_0\rangle} = 120m. \tag{A.32}$$

Subsequently from (A.29)

$$\Theta_2 = -\frac{m\eta^2}{384}(y^6 - 15y^4 + 27y^2), \tag{A.33}$$

and from (A.30)

$$V_2 = \frac{\eta^2(m+1)}{64 \times 6!}(y^6 - 15y^4 + 75y^2 - 61) - \frac{15\eta^2 m}{128 \times 10!}(y^{10} - 45y^8 + 378y^6 - 4455y^2 + 4121) - \frac{T^2}{256 \times 8!}(y^8 - 28y^6 + 350y^4 - 1708y^2 + 1385). \tag{A.34}$$

The order ε^4 equation for Θ is

$$4D_y^2\Theta_4 = s\Theta_0 + m\eta^2\Theta_2 - \eta^2 R_2 V_0 - \eta^2 R_0 V_2 - CV_0. \tag{A.35}$$

From (A.17) and (A.18),

$$\langle D_y^2\Theta_4\rangle = -(b_0 + b_1)/4, \tag{A.36}$$

so upon operating on (A.35) by $\langle\ \rangle$,

$$R_2 = \frac{1}{\eta^2\langle V_0\rangle}(s + b_0 + b_1 + m\eta^2\langle\theta_2\rangle - \eta^2 R_0\langle V_2\rangle - C\langle V_0\rangle) = R_0\left\{\frac{s + b_0 + b_1 - C/120}{m\eta^2} + \left[\frac{34(m+1)}{336} - \frac{31m}{5544}\right]\eta^2 + \frac{31}{3024m}T^2\right\}. \tag{A.37}$$

Therefore the relation between R, σ and a is

$$R = R_0\left[1 + \frac{31\tau^2}{3024m} + \frac{\sigma + \gamma_0 + \gamma_1 - S/120}{ma^2} + \left(\frac{34(m+1)}{336} - \frac{31m}{5544}\right)a^2\right] \tag{A.38}$$

The value of R needed for convective instability increases as a^2 increases and can either increase or decrease as $a^2 \to 0$ depending on the value of $\gamma_0 + \gamma_1 - S/120$.

REFERENCES

Agee, E. M. 1976. Observational evidence of cell flatness as a function of convective depth and eddy anisotropy. *J. Meteorol. Soc. Japan 54*, 68–71.

Agee, E. M. and Dowell, K. E. 1974. Observational studies of mesoscale cellular convection. *J. Appl. Meteorol. 13*, 46–53.

Agee, E. M. and Lomax, F. E. 1978. Structure of the mixed layer and inversion layer associated with patterns of mesoscale cellular convection during AMTEX 75. *J. Atmos. Sci. 35*, 2281–2301.

Atkinson, B. W. 1981. *Mesoscale atmospheric circulations*. Academic Press, 495 pp.

Busse, F. H. 1978. Nonlinear properties of thermal convection. *Rep. Prog. Phys. 41*, 1929–1967.

Busse, F. H. and Riahi, N. 1980. Nonlinear convection in a layer with nearly conducting boundaries. *J. Fluid Mech. 96*, 243–256.

Chandrasekhar, S. 1961. *Hydrodynamic and hydromagnetic stability*. Dover, 652 pp.

Deardorff, J. W. 1976. On the entrainment rate of a stratocumulus-topped mixed layer. *Q. J. R. Meteorol. Soc. 102*, 563–582.

Fiedler, B. H. 1984. The mesoscale stability of entrainment into cloud-topped mixed layers. *J. Atmos. Sci. 41*, 92–101.

Garratt, J. R. and Hicks, B. B. 1973. Momentum, heat and water vapour transfer to and from natural and artificial surfaces. *Q. J. R. Meteorol. Soc. 99*, 680–687.

Hurle, D. T. J., Jakeman, E. and Pike, E. R. 1967. On the solution of the Benard problem with boundaries of finite conductivity. *Proc. R. Soc. A 296*, 469–475.

Jensen, N. O. and Lenschow, D. H. 1978. An observational investigation of penetrative convection. *J. Atmos. Sci. 35*, 1924–1933.

Kraus, H. and Schaller, E. 1978. A note on the closure in Lilly-type inversion models. *Tellus 30*, 284–288.

Krueger, A. F. and Fritz, S. 1961. Cellular cloud patterns revealed by TIROS I. *Tellus 13*, 1–7.

Liu, W. T., Katsaros, K. B. and Businger, J. A. 1979. Bulk parameterization of air-sea exchanges of heat and water vapor including the molecular constraints at the interface. *J. Atmos. Sci. 36*, 1722–1735.

Nayfeh, A. 1973. *Perturbation methods*. Wiley, 425 pp.

Palm, E. 1975. Nonlinear thermal convection. *Ann. Rev. Fluid Mech. 7*, 39–61.

Priestley, C. H. B. 1962. The width-height ratio of large convection cells. *Tellus 14*, 123–124.

Randall, D. A. 1984. Stratocumulus cloud deepening through entrainment. *Tellus 36A*, 446–457.

Ray, D. 1965. Cellular convection with nonisotropic eddys. *Tellus 17*, 434–439.

Rosmond, T. E. 1973. Mesoscale cellular convection. *J. Atmos. Sci. 30*, 1392–1409.

Rothermel, J. and Agee, E. M. 1980. Aircraft investigation of mesoscale cellular convection during AMTEX 75. *J. Atmos. Sci. 37*, 1027–1040.

Sasaki, Y. 1971. Influences of thermal boundary layer on atmospheric cellular convection. *J. Meteorol. Soc. Japan 48*, 492–502.

Sheu, P. J. and Agee, E. M. 1977. Kinematic analysis and air-sea heat flux associated with mesoscale cellular convection during AMTEX 75. *J. Atmos. Sci. 34*, 793–801.

Sparrow, E. M., Goldstein, R. J. and Jonsson, V. K. 1964. Thermal instability in a horizontal fluid layer: effect of boundary conditions and non-linear temperature profile. *J. Fluid Mech. 18*, 513.

Spiegel, E. A. 1971. Convection in stars, I. Basic Boussinesq convection. *Ann. Rev. Astron. Astrophys 10*, 323–352.

Stull, R. B. 1976. The energetics of entrainment across a density interface. *J. Atmos. Sci. 33*, 1260–1267.

van Delden, A. and Oerlemans, J. 1982. Grouping of clouds in a numerical cumulus convection model. *Beitr. Phys. Atmos. 55*, 239–252.

Williams, G. P. 1972. Friction term formulation and convective instability in a shallow atmosphere. *J. Atmos. Sci. 29*, 870–876.

Willis, G. E., Deardorff, J. W. and Sommerville, R. C. J. 1972. Roll-diameter dependence in Rayleigh convection and its effect upon the heat flux. *J. Fluid Mech. 54*, 351–367.